Dhaka Univ. J. Sci. 74(1): 54-61, 2026 (January)
Prof. M. Muhibur Rahman Memorial Issue
ISSN 1022 - 2502, E-ISSN 2408- 8528
DOI: https://doi.org/10.3329/dujs.v74i1.86736

Surfactant-Directed Modulation of SBA 15: Insights into Surface Area, Porosity, and Morphology

Farhana Afroze[1,2,3], Tanvir Ahmed[2,4], Newaz Mohammed Bahadur[3], Md. Abu Bin Hasan Susan[2,5*], and Saika Ahmed[2*]

[1]*Department of Chemistry, Gono Bishwabidyalay, Nolam, Ashulia, Savar, Dhaka-1344, Bangladesh*
[2]*Department of Chemistry, Faculty of Science, University of Dhaka, Dhaka-1000, Bangladesh*
[3]*Department of Applied Chemistry and Chemical Engineering,Noakhali Science and Technology University, Sonapur, Noakhali-3814, Bangladesh*
[4]*Institute of Nuclear Science and Technology, Bangladesh Atomic Energy Commission, Dhaka-1349, Bangladesh*
[5]*Dhaka University Nanotechnology Center, University of Dhaka, Dhaka-1000, Bangladesh*

(Received : 1 October 2025; Accepted : 29 December 2025)

Abstract

Mesoporous silica now-a-days has emerged as a versatile material for nanotechnology and many other applications because of its high surface area and ordered pore architecture. However, careful tuning of synthesis parameters to maximize porosity and surface area is crucial for achieving optimal performance. In this work, SBA 15 type mesoporous silica was synthesized via sol-gel method, using a non-ionic surfactant Pluronic P-123 as the structure-directing template and tetraethyl orthosilicate as the silica precursor. The concentration of surfactant template was systematically varied from 500 to 2500 times its critical micellar concentration (i.e. 0.002 mM). Synthesized SBA 15 samples were then characterized by N_2 adsorption-desorption analysis to evaluate the surface area, pore size, and pore volume, Fourier-transform infrared spectroscopy for structural confirmation, and scanning electron microscopy (SEM) and transmission electron microscopy (TEM) for morphological evaluation. SEM and TEM images indicated that increasing P-123 concentration led to a transition toward cylindrical morphologies, more regular particle size, and improved particle yield, while N_2 adsorption isotherms revealed larger pore diameters and higher surface areas. The results obtained emphasize the critical role of surfactant concentration for tailoring the structural and textural properties of SBA 15, thereby offering useful suggestions for its application in catalysis, adsorption, and drug delivery.

Keywords: Mesoporous silica, SBA 15, Sol-gel synthesis, Pluronic P-123, Surfactant template, Surfactant concentration

I. Introduction

Over the past few years, the scientific world has accepted mesoporous silica as a major material in nanotechnology, primarily because of its unique structure and extensive porosity giving rise to its remarkably high surface area[1]. Such characteristics make it very suitable for applications in drug delivery, imaging, and catalysis[2-14].The first breakthrough came with the M41S family, namely MCM-41, MCM-48, and MCM-50, synthesized by the Mobil Corporation scientists in 1992[15]. Another important class is the SBA (Santa Barbara Amorphous) series, which includes SBA 3, SBA 15, and SBA 16[16]. Among these, SBA 15, introduced by Zhao et al. in 1998[17], has gained special attention due to its high surface area, biocompatibility, nontoxicity, well-defined pore structure, and remarkable thermal and hydrothermal stability[18-20]. Owing to these properties, SBA 15 is widely used in adsorption, drug delivery, sensing, immobilization, catalysis, etc.[21-24].

Mesoporous materials are generally synthesized via template-assisted methods, where surfactants direct the formation of ordered pore structures[25,26]. Surfactants-cationic, anionic, or nonionic- act as structure-directing agents in the synthesis of mesoporous silica. Nonionic surfactants such as amphiphilic block copolymers like alkyl poly(oxyethylene) are particularly useful for their low-cost, nontoxicity, commercial availability, and are widely applied in household, pharmaceutical, emulsifying, and coating industries[27-28]. Their mesostructure-directing ability can also be tuned by factors like copolymer architecture or solvent conditions[17].

SBA 15 is best known for its amazing hexagonal arrangement of cylindrical pores, usually ranging between 5 and 30 nm in diameter[29,30.] To fabricate this structure, triblock copolymer Pluronic P-123 ($EO_{20}PO_{70}EO_{20}$) is often used[22,31]. The self-organization of P-123 into micelles in acidic or basic solutions[22] is a crucial step as such micelles act as the "blueprint" around which silica frameworks form. Beyond the critical micelle concentration (CMC) of P-123, adding more surfactant not only increases the number of micelles but can also alter their micelle aggregation, packing density, and change shape, which in turn can significantly influence the final pore architecture of SBA 15.

The morphology and textural features of SBA 15 particles are dependent on multiple synthesis parameters such as synthesis temperature, aging time, pH, surfactant concentration, etc. For example, increasing the aging temperature and time enlarges the mesopores of SBA 15 while decreasing the surface area[32-35]. Lowering pH causes longer rod-shaped SBA 15 with more stable mesopores[36]. Studies on the variation of surfactant concentration show that increasing the concentration of P-123 increases the specific surface area with increase in pore diameter[37]. Nonetheless, a

*Author for correspondence. e-mail: susan@du.ac.bd, saika@du.ac.bd

few important aspects on SBA 15 are yet to be clarified, e.g. the transformation in pore connectivity and hysteresis with the increase in P-123 and the evolution in the particle assembly from micelles to rods and then to interconnected networks as the synthesis conditions are transformed. To our knowledge, no research has thoroughly studied and illustrated the entire progression of mesostructure, most importantly, the development from micropores to ink-bottle pores and then to open cylindrical pores, as a function of surfactant concentration while keeping the other conditions constant. Thus, an intensive and systematic study of P-123 concentration is scientifically desired. While some studies have demonstrated that P-123 acts as a reliable structure-directing agent, most reports have focused on its general effectiveness rather than quantitatively addressing how its concentration fine-tunes the mesostructure. Addressing this knowledge gap is necessary for modification of SBA 15 for applications in various fields like catalytic reactions, adsorption, or drug delivery, as the effectiveness of all those applications is very much dependent on the surface attributes. The present work thus aims to bridge this gap by systematically investigating the effect of P-123 concentration on the surface area, pore structure, and morphology of SBA 15, thereby identifying the conditions that yield the most favorable textural properties. The goal was also to identify the surfactant concentration that produces the finest structured and most efficient form of mesoporous silica.

II. Materials and Methods

Synthesis of SBA 15

Nonionic surfactant, pluronic P-123 from Sigma Aldrich was used as the structure-directing template for the synthesis of SBA 15. For silica precursor, tetraethyl orthosilicate (TEOS), received from Merck, was employed. SBA 15 was synthesized following a modified Stöber method[17,22] using five different concentrations of P-123, ranging from 500-2500 times its CMC (i.e. 0.002 mM), as the pore and structure-directing agent. Although there is a possibility that enhanced amounts of P-123 could increase the surface area even more, the amount of P-123 was limited to 2500 x CMC in this study, because earlier studies suggested that excessive surfactant can lead to irregular pores being formed, or even collapse of the mesostructure in some cases. The description and sample codes of the synthesized SBA 15 in this work are summarized in Table 1.

Table 1. Sample code and concentration of P-123 for synthesizing SBA 15 samples (Concentration of P − 123 = x × CMC (mM);x is the multiplication factor).

Sample Code	x
SBA 15 (500)	500
SBA 15 (1000)	1000
SBA 15 (1500)	1500
SBA 15 (2000)	2000
SBA 15 (2500)	2500

In order to prepare SBA 15, pre-calculated amounts of P-123 were dissolved in 150.0 g of 1.6 M HCl solution with stirring at 35 ^{o}C for achieving the desired concentration of P-123 in the final solution. 8.5g of TEOS was then added dropwise into this solution with stirring at 35 ^{o}C. The mixture was then allowed to age by heating, first at 35 and then at 100 ^{o}C, for two days without stirring. The aged mixture was filtered, followed by washing with water several times to ensure the removal of Cl^- ions, and the solid silica sample thus obtained was dried overnight at 110 ^{o}C in an oven. Finally, SBA 15 silica was obtained after calcination of the sample at 560 ^{o}C for 10.5 h.

Characterization of SBA 15 samples

Fourier Transform InfraRed (FTIR) spectrophotometry (Frontier FTIR/NIR, Perkin Elmer, USA) was employed for functional group analysis of the synthesized SBA 15 by making its pellets with KBr. The FTIR spectra were recorded in the wavenumber range 4000-400 cm^{-1}. Morphology of the SBA 15 samples was analyzed by Scanning Electron Microscopy (SEM) (Model JSM-6490LA). The SEM images of the solid SBA 15 were taken at an accelerating voltage of 20 KV with magnifications ranging from 10000-50000. The particle size and morphology of the SBA 15 samples were also studied by High Resolution Transmission Electron Microscopy (HRTEM) on a Zeiss EM 912 Ω instrument (acceleration voltage = 120 kV). The image processing and determination of particle size and size distribution from HRTEM measurements were carried out using Image J software (NIH, USA). First, the scale bar was used to calibrate the TEM images. Then the individual particles were measured either by tracing the area of their projection or by their Feret diameter. The measurements were carried out on several particles in various parts of the micrographs to produce a statistically reliable result. The mean ± standard deviation represented the average particle size and size distribution. Surface area, pore volume, and pore size distribution of the synthesized SBA 15 were determined using N_2 adsorption-desorption (BET) analysis (Belsorp mini-II, BEL, Japan). This analysis was performed at -196 ^{o}C using liquid nitrogen as the cryogenic fluid; about 0.025 g of sample was pre-treated at 120 ^{o}C for 3 h and used for each measurement. The surface area of each sample was calculated from their respective BET plots.

II. Results and Discussion

FTIR Spectroscopic Analysis

The FTIR spectra of the SBA 15 samples synthesized using different concentrations of Pluronic P-123 template were recorded in the wavenumber range of 4000-400 cm^{-1} in order to identify the different kinds of bonds/functional groups present. The FTIR spectra of the SBA 15 samples are shown in **Fig. 1**.

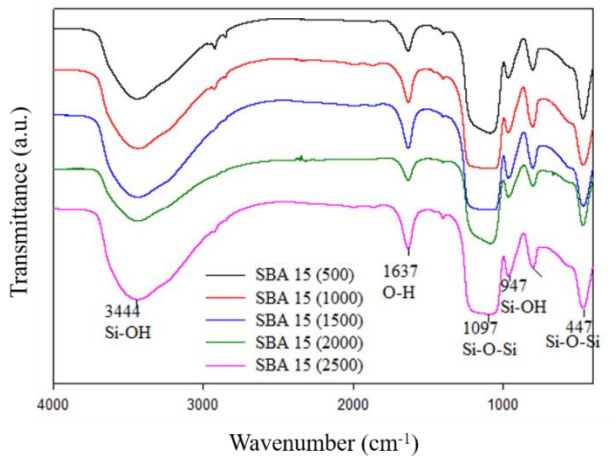

Fig. 1. FTIR spectra of SBA 15 synthesized from five different concentrations of P-123 ([P-123]=x*CMC; x= 500-2500).

FTIR spectra of all the SBA 15 silica samples, synthesized using different concentrations of P-123, exhibit similar patterns in their FTIR spectra. All of them show the characteristic band for Si-O-Si stretching vibration at 447 cm^{-1}. The broad band at around 3444 cm^{-1} corresponds to the stretching vibration comingale from surface silanol (Si-OH) groups. The bending mode of vibration for the silanol O-H groups is observed at around 1637 cm^{-1}. The narrow band at 947 cm^{-1} is attributed to the stretching vibration of Si-OH. Another convoluted band for the stretching vibrations of Si-O-Si group is found in between 1097-805 cm^{-1}.

SEM and TEM Image Analysis

SEM images of the SBA 15 silica samples synthesized at different P-123 concentrations are shown in **Fig. 2,** illustrating the evolution of particle morphology as a function of surfactant concentration. The images represent the surface morphology and size of the silica particles synthesized using five different multiples of the CMC of P-123.

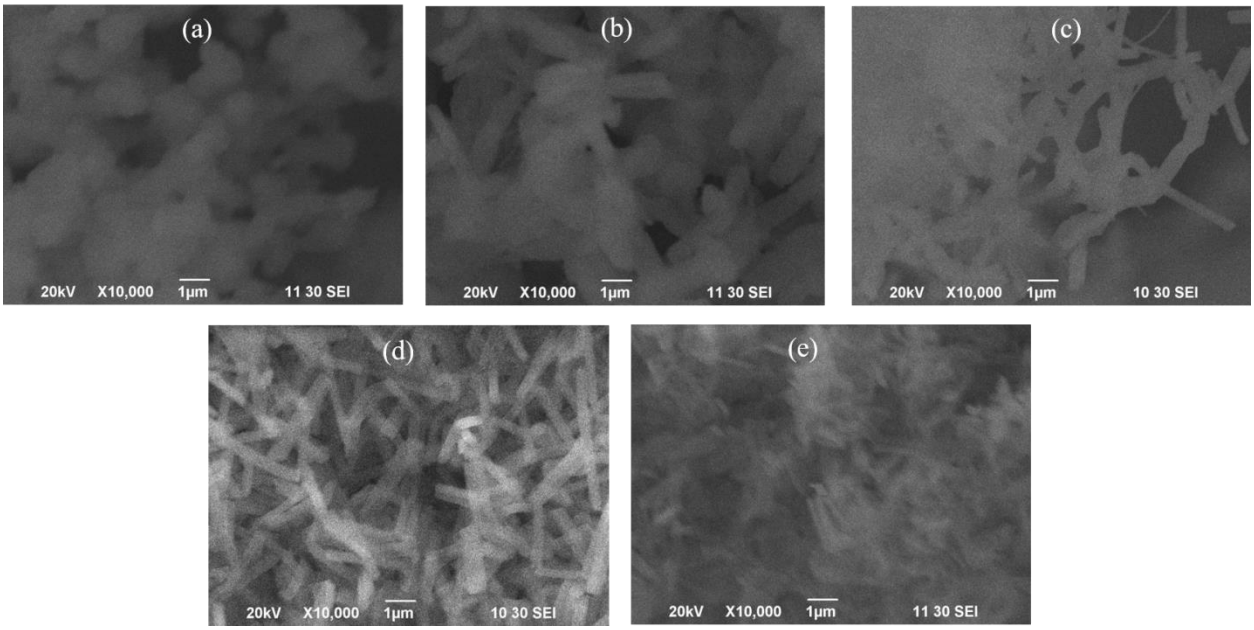

Fig. 2. SEM images of **(a)** SBA 15 (500), **(b)** SBA 15 (1000), **(c)** SBA 15 (1500), **(d)** SBA 15 (2000), and **(e)** SBA 15 (2500), synthesized from different concentrations of P-123.

At the lowest surfactant concentration, SBA 15 (500) did not exhibit any regular morphology, lacking well-defined spherical or cylindrical shapes. As the P-123 concentration increased to 1000×CMC, (SBA 15 (1000)), the particles began to adopt cylindrical morphologies, although with relatively low aspect ratios (**Fig. 2b**). Further increase to 1500×CMC (SBA15 (1500)) led to highly elongated, entangled, noodle-like cylindrical particles with increased aspect ratio (**Fig. 2c),** suggesting a transitional regime of micelle reorganization and silica condensation.

At higher surfactant concentrations, SBA 15 (2000) and SBA 15 (2500) displayed progressively uniform and shorter cylindrical particles (**Figs. 2d and e**), with SBA 15 (2500) exhibiting the clearest defined morphology. This evolution is a direct outcome of the distribution of a constant amount of the silica precursor (TEOS) on the surface of increased number of micellar templates. As micelle number increases as a result of increasing P-123 concentration, the available silica precursor per micelle decreases, limiting longitudinal growth and leading to earlier termination of particle elongation. In addition, since silica condensation proceeds radially outward from the micelle-water interface, at high micelle densities, radial framework thickening dominates while axial growth is sterically constrained. This combined

effect produces shorter, more numerous particles with better-defined pore walls for SBA 15 (2500). Overall, increasing P-123 concentration promotes the transformation from disordered particle morphologies to more uniform and refined cylindrical mesostructures.

The interpretations from SEM image analysis were further supported by HRTEM observations as shown in **Fig. 3.** SBA 15 (500) displays irregular internal features (**Fig. 3a**) which is consistent with its SEM images. SBA 15 (1500), synthesized from an intermediate value of surfactant concentration, exhibits particles with internal pore ridges. A closer examination reveals that the pore walls are irregular in shapes, not clearly defined, and much less uniform (**Fig. 3b**). On the contrary, SBA 15 (2500) particles appear to have clearer and regularly arranged pore channels with improved structural definitions (**Fig. 3c**). In addition, widening of pores along with better pore-wall uniformity are clearly observed at higher P-123 concentration. This gives rise to increased total pore volume and reduction in particle size as observed from SEM analysis, which is expected to result in increased specific surface area.

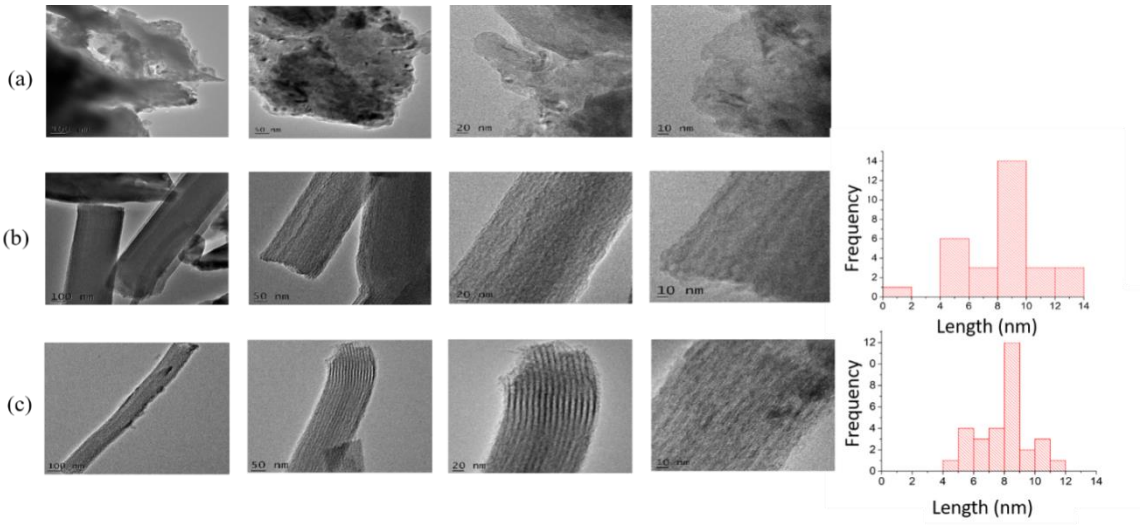

Fig. 3. HRTEM images of (a) SBA 15 (500), (b) SBA 15 (1500), and (c) SBA 15 (2500). The particle size distribution is shown in the right-side figures. The distribution of the particles of SBA 15 (500) could not be analyzed due to irregular particle shapes.

These findings are indicative of the fact that the amount of surfactant template used has a significant and crucial impact on directing the morphology of SBA 15 and thus lies the importance of optimizing surfactant concentration for obtaining SBA 15 particles with uniform mesostructures.

N_2 Adsorption-Desorption Analysis

The variation in concentration of Pluronic P-123, which produces micelles and acts as a pore-directing template in SBA 15, is believed to have a significant impact on the surface properties of SBA 15, mainly the surface area and pore structure. These effects were examined using N_2 adsorption–desorption measurements. The corresponding isotherms and BJH pore size distribution plots for the synthesized samples are presented in **Fig. 4**.

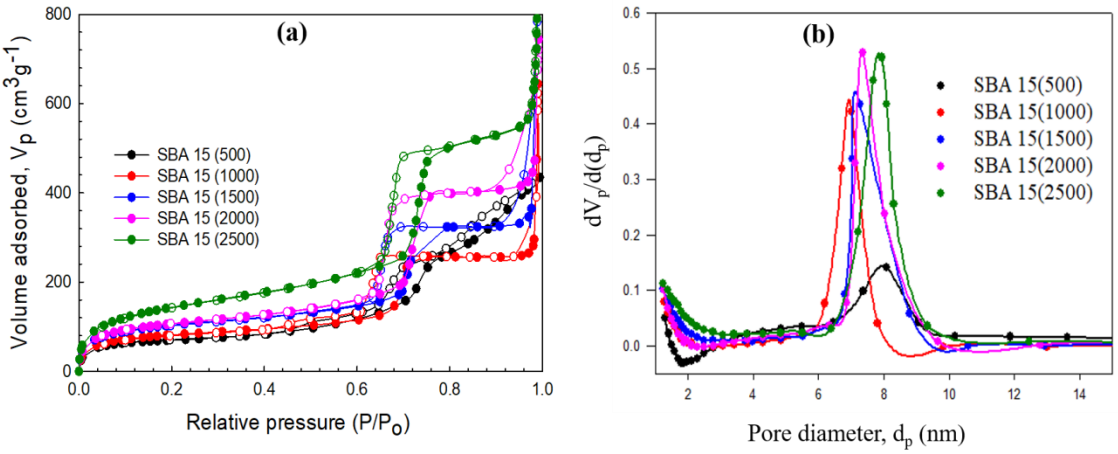

Fig. 4. **(a)** N_2 adsorption-desorption isotherms and **(b)** BJH pore size distribution curves (analyzed from the adsorption branch) of SBA 15 synthesized using five different concentrations of P-123.

As shown in **Fig. 4(a)**, all isotherms of SBA 15 samples exhibited Type IV isotherm according to the IUPAC classification [38], confirming their mesoporous nature. The hysteresis loops of the adsorption-desorption isotherms appeared in the relative pressure (P/P_o) range of 0.5-0.8, which is characteristic of capillary condensation inside mesopores. Both the shape and symmetry of the hysteresis loops varied markedly with P-123 concentrations, indicating differences in pore geometry and connectivity.

The SBA 15 (500) sample exhibited a poorly defined hysteresis loop with features resembling weak H4-type behavior at higher relative pressures, which is typically associated with slit-like or structurally disordered pores [38,39] This is indicative of poor mesopore organization and limited connectivity between the pore, also consistent with the irregular morphology and underdeveloped internal porosity observed in the SEM and TEM analyses. On the other hand, a distinct H2-type hysteresis loop exhibited by SBA 15 (1000) is characteristic of ink-bottle-type pore systems with narrow pore necks being connected to larger cavities, which indicates poor accessibility towards inside the pores. When the surfactant concentration is at an intermediate level, SBA 15 (1500) exhibits a transition of hysteresis pattern from H2 to H1-types, indicating partial rearrangement of the pores and as low transformation from irregular slit-type mesopores to cylindrical mesoporous channels. Further increase in P-123 concentration show more symmetric and defined H1-type hysteresis loops (i.e. SBA 15 (2000) and SBA 15 (2500)), which results from increased regularity in the shape of cylindrical pores and better pore connectivity and structural regularity. Among all the samples, SBA 15 (2500) exhibits the highest N_2 uptake and the largest hysteresis loop (**Fig. 4a**), confirming the formation of a highly ordered and well-developed mesoporous framework.

The BJH pore size distribution curves for all the SBA 15 samples as shown in **Fig. 4(b)** exhibit well-defined peaks in the range of 6 to 10 nm, indicating the presence of mesopores. Except SBA 15 (500), all the SBA 15 samples reveal an increase in pore diameter from 7.02 to 7.93 nm with increasing concentration of P-123.

Analysis of the adsorption-desorption isotherms and corresponding BET and BJH plots provided the specific surface area, total pore volume, and mean pore diameter of the silica samples synthesized from different P-123 concentrations. The values of these parameters are summarized in **Table 2** and the variation is graphically shown in **Fig. 5**.

Table 2. BET specific surface area, total pore volume, and mean pore diameter of SBA 15 silica nanoparticles synthesized from different concentrations of P-123 surfactant templates.

SBA 15 Sample	Specific surface area (m^2g^{-1})	Total pore volume (cm^3g^{-1})	Mean pore diameter (nm)
SBA 15 (500)	265	0.61	8.07
SBA 15 (1000)	306	0.98	7.02
SBA 15 (1500)	384	0.56	7.27
SBA 15 (2000)	400	0.73	7.35
SBA 15 (2500)	529	1.49	7.93

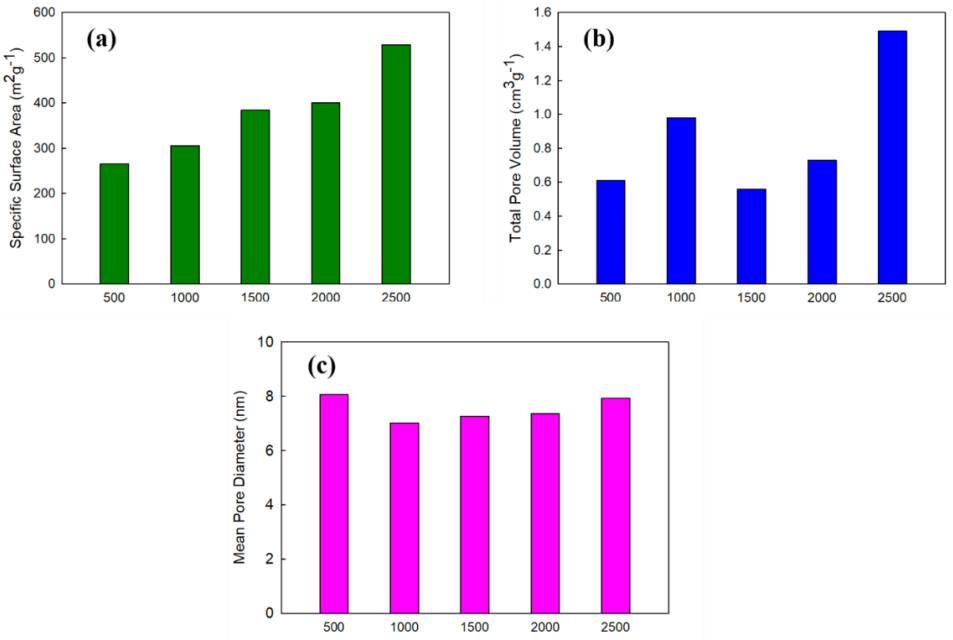

Fig. 5. Variation of **(a)** surface area, **(b)** total pore volume, and **(c)** mean pore diameter of the five SBA 15 samples, determined from N_2 adsorption-desorption analysis.

The specific surface area (BET) (**Fig. 5a**) increases monotonically with increasing P-123 concentration, reflecting the combined effects of enhanced internal pore surface development along with a progressive reduction in particle size also observed in SEM analysis. In contrast, the total pore volume (**Fig. 5b**) exhibits a non-monotonic trend, with an increase from SBA 15 (500) to SBA 15 (1000), then decrease at SBA 15 (1500), and then again progressive increase toward SBA 15 (2500). This difference arises because surface area and pore volume respond differently to structural evolution; surface area is affected by roughness of pore walls and external particle surface and particle shapes, whereas pore volume depends primarily on the presence of fully open, well-connected mesoporous channels. For SBA 15 (1500), the increased number density of micellar templates probably leads to incomplete pore development and local constrictions during the H2→H1 hysteresis transition, thus temporarily restricting accessible mesoporous void volume despite continued surface area growth. Therefore, SBA 15 synthesized at an intermediate P-123 concentration (1500×CMC) represents a „transitional mesostructural regime" rather than a fully developed SBA 15 framework. At higher P-123 concentrations, improved micelle ordering and framework regularization establish the proportional relationship between surface area and pore volume. The influence of P-123 concentration on the evolution of particle shape and morphology and pores of SBA 15 is schematically represented in **Scheme 1**.

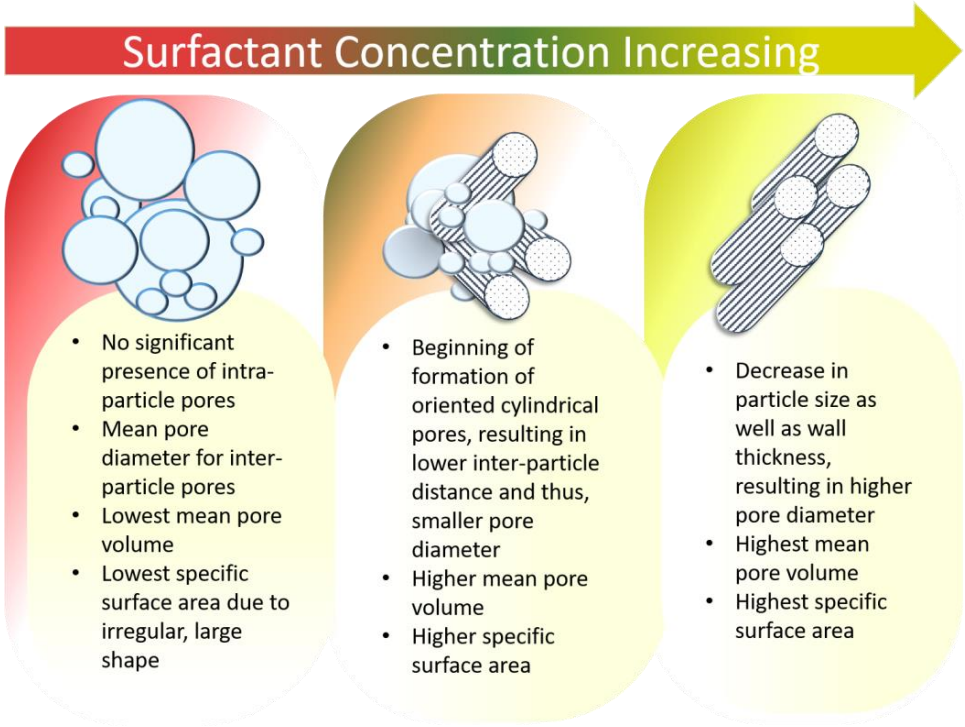

Scheme 1: Schematic illustration explaining the variation of size and morphology of SBA 15 particles and their pores, synthesized from different concentrations of Pluronic P-123.

IV. Conclusions

SBA-15 mesoporous silica was systematically synthesized by sol-gel method using varying concentrations of the nonionic surfactant Pluronic P-123 to elucidate the effect of micelle packing on the tuning of particle structure and pore evolution. FTIR spectroscopic analysis confirmed the silica network, and SEM and TEM image analysis revealed clear morphological evolution with increasing surfactant concentration, where the particles became more distinct, smaller, and well-ordered at higher P-123 concentration. Nitrogen adsorption-desorption analysis demonstrated that the surface area and pore characteristics of SBA 15 are strongly influenced by the concentration of P-123. The surface area increased with rising surfactant concentration monotonously, while pore diameter generally increased except at the lowest concentration (SBA 15 (500)). Overall, the findings highlight the critical role of surfactant concentration in tailoring the textural and morphological properties of SBA 15. The outcome of the study indicates that a strategic regulation of the P-123 concentration leads to adjustable particle shape and mesoporous structure which, in turn, offers a logical way to improve the SBA 15 materials for those applications where high surface area, ordered porosity, and efficient mass transport are required.

Acknowledgements

The authors acknowledge Bose Centre for Advanced Study and Research in Natural Sciences for offering research fellowship and providing financial support to the first author. The University Grants Commission (UGC) of Bangladesh is gratefully acknowledged for providing a research grant. The authors also acknowledge Sophisticated Test and Instrumentation Centre, India, for support in the analytical services for the HRTEM studies.

References

1. Fedeyko, J.M., D.G. Vlachos, and R.F. Lobo, 2006. Understanding the Differences between Microporous and Mesoporous Synthesis Through the Phase Behavior of Silica. *Microporous Mesoporous Mat*. **90**, 102-111.
2. Trewyn, B.G., J.A. Nieweg, Y. Zhao, and V.S.-Y. Lin, 2007. Biocompatible Mesoporous Silica Nanoparticles with Different Morphologies for Animal Cell Membrane Penetration. *Chem. Eng. J*. **137(1)**, 23–29.
3. Sooyeon, K, R.K. Singh, and C. Wojciech, 2013. Silica-Based Mesoporous Nanoparticles for Controlled Drug Delivery. *J. Tissue Eng.* 4, 1-35.
4. Brannon-Peppas, L., 1995. Recent Advances on the Use of Biodegradable Microparticles and Nanoparticles in Controlled Drug Delivery. *Int. J. Pharm.* **116(1)**, 1-9.
5. Tourne-Peteilh, C., S. Begu, D.A. Lerner, A. Galarneau, U. Lafont and J.M. Devoisselle, 2012. Sol-Gel One-Pot Synthesis in Soft Conditions of Mesoporous Silica Materials Ready for Drug Delivery System. *J. Sol-Gel Sci. Technol.* **61**, 455-462.
6. Liong, M, J. Lu, M. Kovochich, T. Xia, S.G. Ruehm, A.E. Nel, F. Tamanoi, and J.I. Zinket, 2008. Multifunctional Inorganic Nanoparticles for Imaging, Targeting, and Drug Delivery. *ACS Nano* **2(5)**, 889–896.
7. Shi, L.-Y., Y.-X. Li, D.-M. Xue, P. Tan, Y. Jiang, X.-Q. Liu and L.-B. Sun, 2020. Fabrication of Highly Dispersed Nickel in Nanoconfined Spaces of As-Made SBA-15 for Dry Reforming of Methane with Carbon Dioxide. *Chem. Eng. J*. 390, 124491.
8. Yin, Y., P. Tan, X.-Q. Liu, J. Zhu and L.-B. Sun, 2014. Constructing A Confined Space in Silica Nanopores: An Ideal Platform for the Formation and Dispersion of Cuprous Sites. *J. Mater. Chem. A* **2(10)**, 3399-3406.
9. Singh, S., R. Kumar, H.D. Setiabudi, S. Nanda, S. and D.-V.N. Vo, 2018. Advanced Synthesis Strategies of Mesoporous SBA-15 Supported Catalysts for Catalytic Reforming Applications: A State-of-the-Art Review. *Appl. Catal. A-Gen*. 559, 57-74.
10. Singh R.K., K.D. Patel, K.W. Leong, and H.-W. Kim, 2017. Progress in Nanotheranostics Based on Mesoporous Silica Nanomaterial Platforms. *ACS Appl. Mater. Interfaces* 9(12), 10309–10337.
11. Tao, Z. 2014. Mesoporous Silica-Based Nanodevices for Biological Applications. *RSC Adv*. **4(36)**, 18961–18980.
12. Li, Z., J.C. Barnes, A. Bosoy, J.F. Stoddart, and J.I. Zink, 2012. Mesoporous Silica Nanoparticles in Biomedical Applications. *Chem. Soc. Rev.* **41(7)**, 2590–2605.
13. Daksh, S., P. Bose, N. Kumar, H. Ojha, S. Deep, and A. Datta, 2025. Mesoporous Silica Nanoparticles for Targeted $A\beta_{42}$ Imaging and Therapy in Traumatic Brain Injury: Enhanced Blood–Brain Barrier Penetration and Sustained Drug Delivery. *ACS Appl. Nano Mater*. **8(22)**, 11322–11337.
14. Chung, T., S. Wu, M. Yao, C. Lu, Y. Lin, Y. Hung, C. Mou, Y. Chen, and D. Huang, 2007. The Effect of Surface Charge on the Uptake and Biological Function of Mesoporous Silica Nanoparticles in 3T3-L1 Cells and Human Mesenchymal Stem Cells. *Biomater.* **28(19)**, 2959-2966.
15. J.C. Vartuli, W.J. Roth, and T.F. Degnan, 2008, Mesoporous materials (M41S): From discovery to application, In Dekker Encyclopedia of Nanoscience and Nanotechnology, J.A. Schwarz, C.I. Contescu, and K. Putyera (Eds.), Marcel Dekker, Inc., New York, 1797-1811.
16. Katiyar, A., S. Yadav, P.G. Smirniotis, and N.G. Pinto, 2006. Synthesis of Ordered Large Pore SBA-15 Spherical Particles for Adsorption of Biomolecules. *J. Chromatogr. A* **1122(1–2)**, 13–20.
17. Zhao, D., Q. Huo, J. Feng, B.F. Chmelka, and G.D. Stucky, 1998. Nonionic Triblock and Star Diblock Copolymer and Oligomeric Surfactant Syntheses of Highly Ordered, Hydrothermally Stable, Mesoporous Silica Structures. *J. Am. Chem. Soc*. **120(24)**, 6024–6036.
18. Zhao, W., J. Gu, L. Zhang, H. Chen, and J. Shi, 2005. Fabrication of Uniform Magnetic Nanocomposite Spheres with A Magnetic Core/Mesoporous Silica Shell Structure. *J. Am. Chem. Soc*. **127(25)**, 8916–8917.
19. Anilkumar, B., S. Sunil, P. Hariharan, R. Yamuna, and N. Pandurangan, 2025. Silica-Based (SBA-15) Sustainable Materials and Their Recent Advances in Biomedical Applications. *Inorg. Chim. Acta* 585, 122766.
20. Shah, P. and V. Ramaswamy, 2008. Thermal Stability of Mesoporous SBA-15 and Sn-SBA-15 Molecular Sieves: An in situ HTXRD Study. *Microporous Mesoporous Mater*. **114(1–3)**, 270-280.
21. Gkiliopoulos, D., I. Tsamesidis, A. Theocharidou, G.K. Pouroutzidou, E. Christodoulou, E. Stalika, K. Xanthopoulos, D. Bikiaris, K. Triantafyllidis, and E. Kontonasaki, 2022. SBA-15 Mesoporous Silica as Delivery Vehicle for rhBMP-2 Bone Morphogenic Protein for Dental Applications. *Nanomaterials* **12(5)**, 822.
22. Zhao, D., J. Feng, Q. Huo, N. Melosh, G.H. Fredrickson, B.F. Chmelka, and G.D. Stucky, 1998. Triblock Copolymer Syntheses of Mesoporous Silica with Periodic 50 to 300 Angstrom Pores. *Science* **279**(5350), 548–552.
23. Guan, M., W. Liu, Y. Shao, H. Huang, and H. Zhang, 2009. Preparation, Characterization and Adsorption Properties Studies of 3-(Methacryloyloxy)Propyltrimethoxysilane Modified and Polymerized Sol–Gel Mesoporous SBA-15 Silica Molecular Sieves. *Microporous Mesoporous Mater*. **123(1-3)**, 193–201.
24. de Sousa, A., D.A. Maria, R.G. de Sousa, and E.M.B. de Sousa, 2009. Synthesis and Characterization of Mesoporous Silica/Poly(N-Isopropylacrylamide) Functional Hybrid Useful for Drug Delivery. *J. Mater. Sci*. **45**, 1478–1486.
25. Lin, V.S.-Y. C.-Y. Lai, J. Huang, S.-A. Song, and S. Xu, 2001. Molecular Recognition Inside of Multifunctionalized Mesoporous Silicas: Toward Selective Fluorescence Detection of Dopamine and Glucosamine. *J. Am. Chem. Soc*. 123(46), 11510–11511.
26. Wang, X., K.S.K. Lin, J.C.C. Chan, and S. Cheng, 2005. Direct Synthesis and Catalytic Applications of Ordered Large Pore Aminopropyl-Functionalized SBA-15 Mesoporous Materials. *J. Phys. Chem. B* **109(5)**, 1763–1769.

27. Meziani, A., D. Tourand, A. Zradba, S. Pulvin, I. Pezron, M. Clausse, and W. Kunz, 1997. Comparison of Enzymatic Activity and Nanostructures in Water/Ethanol/Brij 35 and Water/1-Pentanol/Brij 35 Systems. *J. Phys. Chem. B* **101(18)**, 3620-3625.

28. Tarcha, P.J., 1990. *Polymers for Controlled Drug Delivery*. CRC Press, Taylor & Francis Group. FL.

29. Ravikovitch, P.I. and A.V. Neimark, 2001. Characterization of Micro- and Mesoporosity in SBA-15 Materials from Adsorption Data by the NLDFT Method. *J. Phys. Chem. B* 105(29), 6817–6823.

30. Ruthstein, S., V. Frydman, S. Kababya, M. Landau, and D. Goldfarb, 2003. Study of the Formation of the Mesoporous Material SBA-15 by EPR Spectroscopy. *J. Phys. Chem. B* **107(8)**, 1739–1748.

31. Wanka, G., H. Hoffmann, and W. Ulbricht, 1994. Phase Diagrams and Aggregation Behavior of Poly(Oxyethylene)-Poly(Oxypropylene)-Poly(Oxyethylene) Triblock Copolymers in Aqueous Solutions. *Macromolecules* **27(15)**, 4145–4159.

32. Fulvio, P.F., Pikus, S., and M. Jaroniec, 2005. Tailoring Properties of SBA-15 Materials by Controlling Conditions of Hydrothermal Synthesis. *J. Mater. Chem.* **15(47)**, 5049-5053.

33. Thahir, R., Sofyan, N., and D. Dhaneswara, 2019. Synthesis of Mesoporous Silica SBA-15 through Surfactant Set-up at Various Temperatures. *Rasayan J. Chem.* **12(3)**, 1335–1342.

34. Lu, B., and K. Kawamoto, 2012. Synthesis of SBA-15 Mesoporous Silica under Different Aging Conditions and Its Structural Stability. *Mater. Res. Bull.* **47(7)**, 1689–1696.

35. Kareem, Y.S., Hussein, H.Q., and W.S. Abdul-Majeed, 2024. The Effect of Hydrothermal Conditions on Surface Properties of Synthesized Nano SBA-15 using Sodium Silicate. *Iraqi J. Chem. Pet. Eng.* **25(3),** 153-160.

36. Koh, M.H., Azaman, S.H., Hameed, B.H., and A.M. Din, 2017. Surface Morphology and Physicochemical Properties of Ordered Mesoporous Silica SBA-15 Synthesized at Low Temperature. In *IOP Conference Series: Materials Science and Engineering* **206(1)**, p. 012056). IOP Publishing.

37. Dhaneswara, D., and N. Sofyan, 2016. Effect of Different Pluronic P123 Triblock Copolymer Surfactant Concentrations on SBA-15 Pore Formation. *Int. J. Technol.* **7(6)**, 1009-1015.

38. Thommes, M., K. Katsumi, A.V. Neimer, J.P. Olivier, R. Francisco, R. Jean, and K.S.W. Sing, 2015. Physisorption of Gases, with Special Reference to the Evaluation of Surface Area and Pore Size Distribution (IUPAC Technical Report). *Pure Appl. Chem*. **87(9-10)**, 1051-1069.

39. Keluo, C.H.E.N., Zhang, T., Xiaohui, C.H.E.N., Yingjie, H.E., and X. Liang, 2018. Model Construction of Micro-pores in Shale: A Case Study of Silurian Longmaxi Formation Shale in Dianqianbei Area, SW China. *Pet. Explor. Dev*. **45(3)**, 412-421.